Impact analysis of temporal resolution in thermal signal reconstruction via infrared imaging

Wen-Chin Yang, You-Gang Yang, Yun-Chung Liu, Wei-Min Liu*

Dept. of Computer Science and Information Engineering, National Chung-Cheng University, Taiwan
E-mail: wmliu@cs.ccu.edu.tw Tel: +886-5-2720411 ext. 33100

***Abstract*—Thermal Signal Reconstruction (TSR) is a well-known nondestructive evaluation technique. It enhances the locations of defects in composite materials in aerospace industry, and has been applied in infrared imaging of human hands recently to locate microvasculature under the skin. In this work we reinvestigated the new application and explored the relationship between the temporal resolutions in TSR and the quality of reconstructed images. The goal is to optimize the variable to improve the detection rate of microvasculature under difficult situations.**

I. INTRODUCTION

Visualization of different vessels under human skin is beneficial to further study of local vascular functions and inference of systemic circulatory health. It is still a difficult task to expose the vessels especially microvasculatures. Recently, several methods have been proposed to enhance the contrast between the skin and vessels. Zeman *et al* [1] used near infrared (NIR) light to illuminate the test site and enhance the subcutaneous veins by projecting the observed NIR images right onto the same location. Systems such as AccuVein (AccuVein LLC, Cold Spring Harbor, NY) and Vascular Viewer (IRIS, Bethlehem, PA) also used NIR light to assist human vision on locating veins [2]. In addition to NIR, thermal imaging is another way capable of visualizing vessels with the help of the natural contrast agent, the warm blood from the core body. Although its value in medical applications was controversial when considering the uneven vascular patterns on the breasts as an indicator of potential breast cancers [3], Bagavathiappan *et al* [4] used it to study peripheral vascular abnormalities and achieved good agreement with clinical findings. Gorbach *et al* [5] demonstrated that the skin temperature was correlated with the blood flow by acquiring infrared images from the forearms of patients with sickle cell disease during the vasoactive drug infusion experiment.

Other than applications of different wavelengths, data processing is another track to improve the visibility of vessels. Liu *et al* [6] showed that applying thermal signal reconstruction (TSR) [7] on IR image series could greatly increase the contrast between the skin and vasculatures during reactive hyperemia period in a brachial-artery occlusion test. TSR is a well-known nondestructive evaluation technique used in aerospace industry to detect defects inside a sample. Although the physical model changed from a solid sample to soft tissues on humans, the huge improvement on the contrast motivated us to investigate the relationship between the temporal resolution (i.e. the image acquisition rate) and the performance of contrast enhancement.

This paper is organized as follows. In section II we introduce our data collection procedures, hardware, the preprocessing steps, the TSR method, and the evaluation approaches. Section III showed the experimental results. Finally, we conclude our findings and unsolved problems in section IV.

II. METHODOLOGIES

A. Data Collection

The experiment procedures were approved by Institutional Review Board of National Institutes of Health, USA. The image data was recorded by a calibrated 8-14 μm long wave IR camera (NEC R300W2-NNU, NEC Avio Infrared Technologies Co., Ltd, Japan) with <0.05 ºC temperature sensitivity, 320 x 240 pixels per image, and 14 bits A/D resolution.

Before the start of experiment, a healthy 24-year old male subject has stayed in a temperature-controlled (25ºC) room for at least 30 minutes. A deflated blood pressure cuff was put on the subject's left forearm in advance. The camera was set up at 60 cm above his arm (Fig.1). Regarding to the experimental settings, we recorded images for 2, 3, 4 minutes of arterial occlusion (OC) individually, each with the same baseline (BL) period (2 minutes) and post occlusion (PO) period (2 minutes). There is a 30 minutes break between each occlusion experiment.

Fig. 1 The IR camera and the recorded images.

To study the influence of the temporal resolutions on the visibility of vasculatures after TSR processing, three occlusion experiments were recorded in 20 Hz (20 frame/sec). The datasets were then resampled in 2 Hz, 5 Hz, and 10 Hz. Therefore 12 data sets in total were generated for the study.

B. Preprocessing—Alignment

In order to eliminate the motion artifact, it was necessary to apply the image alignment during the whole imaging period before TSR processing. The first frame served as the reference image to perform rigid-body image registration, where three red areas marked in Fig. 2 were used to compare with other images to find the best fit. The implementation was under MATLAB 7.10 (MathWorks, Inc., USA). Some built-in functions in the Statistical Parametric Mapping Signal Processing Toolbox were used for registration.

To speed up the following TSR processing and discern the different tissues in human's hand easily, a region of interest (ROI) contained only the subjects' forearm was drawn manually by ENVI 4.8 (ITT Industries, Boulder, CO) to exclude background pixels.

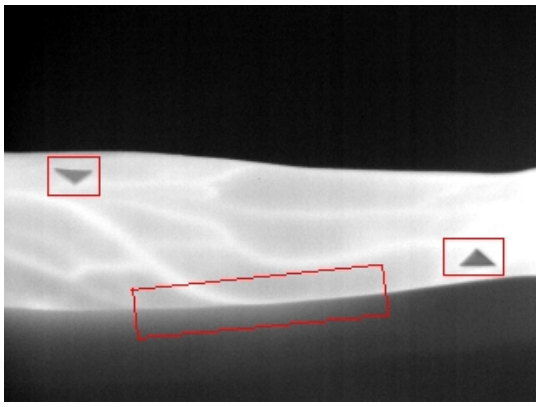

Fig. 2 The ROIs for image alignment.

C. Thermal Signal Reconstruction (TSR)

The TSR method was described in [6, 7]. It hypothesized that given a uniform heating, the heat transfer in a solid sample would follow the one-dimensional heat diffusion equation (1) unless the energy was obstructed by the defect:

$$\frac{\partial^2 T}{\partial z^2} - \frac{1}{\alpha}\frac{\partial T}{\partial t} = 0 \tag{1}$$

The solution of equation (1) is

$$\mathrm{T} = \frac{Q}{e\sqrt{\pi t}} \tag{2}$$

where T stands for the temperature, α stands for the thermal diffusivity, z stands for the vertical direction of the sample, Q stands for the input energy, and e is the thermal effusivity.

For better visualization of the time-evoluted difference on the sample surface temperature and the reduction of temporal noise, a logarithmic representation is commonly adopted. This leads the equation (1) and equation (2) to

$$\ln(T) = \ln\left(\frac{Q}{e}\right) - \frac{1}{2}\ln(\pi t) \tag{3}$$

The TSR method described above was implemented under Matlab with the following steps:

1. All the image cubes recorded by the IR camera were masked (section B) such that only the subject's forearm was left for TSR processing.
2. Extract the pixel vectors (Temperature vs. time) and select the duration corresponding to the first 50 seconds (t_{50}) of the post occlusion (PO) period.
3. The extracted pixel vectors (Temperature vs. t_{50}) were then transformed into the logarithmic domain, i.e. $\ln(T)\ vs.\ln(t_{50})$.
4. Each transformed pixel vector is approximated by a n-order polynomial fitting:

$$\ln[T(t_{50})] = \sum_{n=0}^{N} a_n[\ln(t_{50})]^n \tag{4}$$

5. Reconstruct the data by Equation (5):

$$\mathrm{T}(t_{50}) = exp\left(\sum_{n=0}^{N} a_n[\ln(t_{50})]^n\right) \tag{5}$$

6. Calculate the first, second, or higher order derivative from the reconstructed data. The results were considered as the "derivative profiles".
7. Synthesize all the processed profiles to an image cube for further analysis.

In the 4th step, the 4th order and 5th order polynomial was tested in our study for comparison. We speculate that the lower order polynomial would be less sensitive to the noise. The first derivative images shown in the next section were calculated in the aforementioned 6th and 7th steps.

D. Quantification of Contrast Enhancement

Through TSR processing the low-contrast raw data can be transformed into higher-contrast image series. We believed that higher contrast is helpful in distinguishing vasculatures from the skin. The image contrast was evaluated by the following two measures.

The first measure was proposed by Beghdadi and Negrate [8] and described as follows:

1. For each pixel of the input image $f(\mathrm{x},\mathrm{y})$, compute the edge value denoted by $\nabla f_{(x,y)}$ for all frames in the image cube.
2. For each pixel of the input image $f(\mathrm{x},\mathrm{y})$, define a sliding window denoted by $W_{(i,j)}$ which was of the size

$m \times m$. The size of m should be odd such that the center of the sliding window and the current location can be considered as pixel (i, j). Then the mean edge intensity $\overline{E}_{(i,j)}$ was calculated as

$$\overline{E}_{(i,j)} = \left(\sum_{x,y \in W_{(i,j)}} f(\mathrm{x},\mathrm{y}) \cdot \nabla f_{(x,y)} \right) \Big/ \left(\sum_{x,y \in W_{(i,j)}} \nabla f_{(x,y)} \right) \quad (6)$$

3. The contrast with respect to the pixel (i, j) was defined by

$$C_{(i,j)} = \frac{\left| f_{(i,j)} - \overline{E}_{(i,j)} \right|}{\left| f_{(i,j)} + \overline{E}_{(i,j)} \right|} \quad (7)$$

and should be in the interval of [0,1].

Some details of the implementation are noteworthy. The edge value $\nabla f_{(x,y)}$ in the 1st step can be derived from any kinds of edge detection operator. Here we used Sobel operator in the study. Equation (8) is an example which detects the edges in horizontal directions.

$$\text{Sobel mask for horizontal edges} = \begin{bmatrix} 1 & 2 & 1 \\ 0 & 0 & 0 \\ -1 & -2 & -1 \end{bmatrix} \quad (8)$$

In the 2nd step, the window should be large enough to be less sensitive to the noise. Here we set it as 41×41.

The second contrast measure is Signal to Noise Ratio (SNR), which is a common evaluation tool used in signal processing, multimedia, and image processing. The basic concept is to compare the strength between the desired signal and its reference. The reference can be either noise or a specific background area.

The definition in logarithmic format is defined as:

$$SNR_{\mathrm{db}} = 10 \log_{10} \left(\frac{A_{signal}}{A_{noise}} \right)^2 = 20 \log_{10} \left(\frac{A_{signal}}{A_{noise}} \right) \quad (9)$$

where A_{signal} and A_{noise} are amplitude of signal and noise. It is obvious that the higher signal amplitude would result in greater SNR value and vice versa. In our evaluation A_{signal} was calculated from the microvasculature area, and A_{noise} was derived from a uniform skin area without any visible vasculature patterns.

III. EXPERIMENTAL RESULTS

A. *Experiment 1 — Contrast quantification*

In this experiment, we used equation (7) to calculate the average contrast over two window areas with different sizes, large and small. The window areas were selected to avoid the largest conduit vessel.

I. *Large window on the subject's arm*

Figure 3, 4 and 5 showed the unprocessed IR images with the largest contrast after 2, 3, and 4 minutes occlusion respectively. The contrast was calculated from a red rectangle area marked in figures. The intensity of each set of sub-figures were in the same scale. The unit of the scale bar is temperature in Celsius.

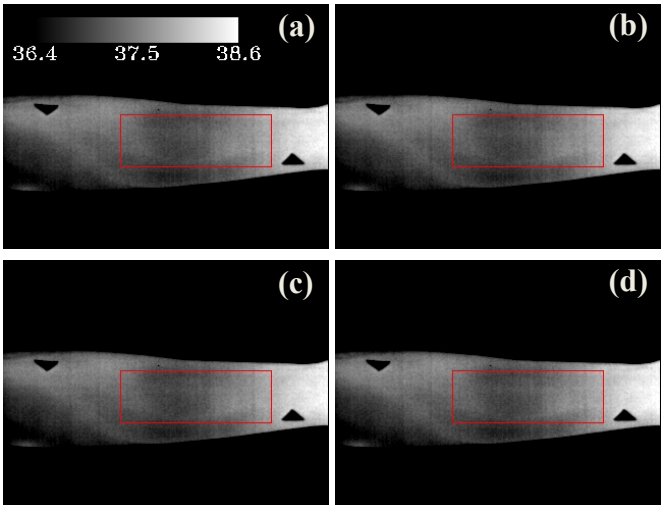

Fig. 3 Frames with the highest contrast after 2 minutes occlusion (a) 2 Hz; (b) 5 Hz; (c) 10 Hz; (d) 20 Hz.

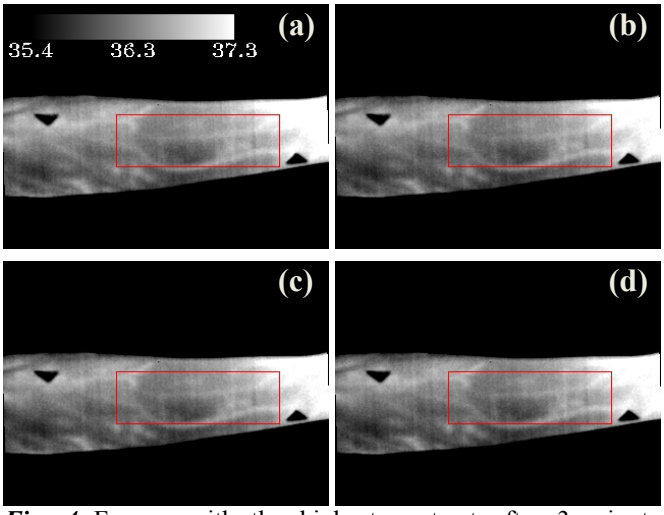

Fig. 4 Frames with the highest contrast after 3 minutes occlusion (a) 2 Hz; (b) 5 Hz; (c) 10 Hz; (d) 20 Hz.

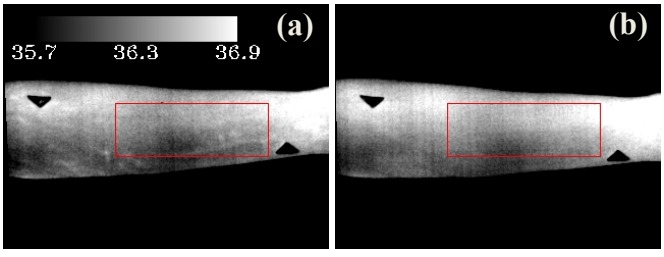

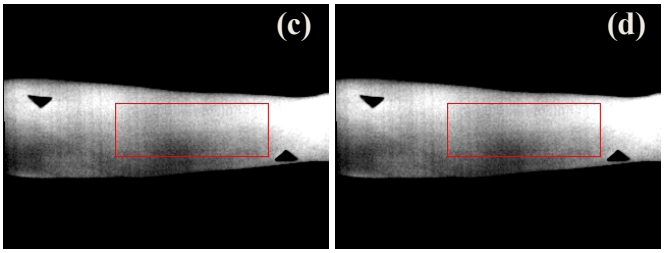

Fig. 5 Frames with the highest contrast after 4 minutes occlusion (a) 2 Hz; (b) 5 Hz; (c) 10 Hz; (d) 20 Hz.

Since image series in 2, 5, and 10 Hz were re-sampled from the original 20Hz sampling rate, the four sub-figures in each experiment were generally similar to each other. The only exception happened in Fig. 5(a) where we can see some slight vascular patterns but not in Fig. 5(b-d). If such image also exists in the other three sampling rates, then we can infer that the contrast measure is sensitive to the noise. The 2nd inconsistency is that Fig. 5 should have clearer vasculature than Fig. 4 and Fig. 3 because 4 minutes occlusion is the strongest physical stimulation, and the subject should have a strong reaction in terms of reactive hyperemia. After re-checking the raw data, we confirmed that the contrast measure did not catch the moment of maximum reactive hyperemia.

Tables 1-3 showed the results of the maximum contrast values and the corresponding frame numbers (inside the parenthesis). The "order" 4 and 5 are the orders used for polynomial fitting.

Table 1 The maximum contrast values and corresponding frame numbers after 2 minutes occlusion.

	Raw data	4th order	5th order
2 Hz	0.4133 (8)	0.9643 (2)	0.9019 (2)
5 Hz	0.4201 (19)	0.9488 (4)	0.9420 (7)
10 Hz	0.4234 (39)	0.9497 (12)	0.9714 (11)
20 Hz	0.4391 (83)	0.9601 (22)	0.9876 (17)

Table 2 The maximum contrast values and corresponding frame numbers after 3 minutes occlusion.

	Raw data	4th order	5th order
2 Hz	0.2751 (96)	0.8319 (67)	0.8437 (70)
5 Hz	0.2821 (219)	0.8209 (48)	0.8871 (5)
10 Hz	0.2821 (438)	0.8153 (94)	0.8884 (7)
20 Hz	0.2910 (879)	0.8572 (2)	0.8794 (9)

Table 3 The maximum contrast values and corresponding frame numbers after 4 minutes occlusion.

	Raw data	4th order	5th order
2 Hz	0.2307 (36)	0.9006 (9)	0.9677 (6)
5 Hz	0.2433 (28)	0.9716 (15)	0.9720 (10)
10 Hz	0.2433 (56)	0.9869 (23)	0.9673 (17)
20 Hz	0.2433 (112)	0.9836 (41)	0.9462 (29)

After TSR processing, reconstructed differential images (TSR-image) with the clearest contrast were shown in Figure 6-11.

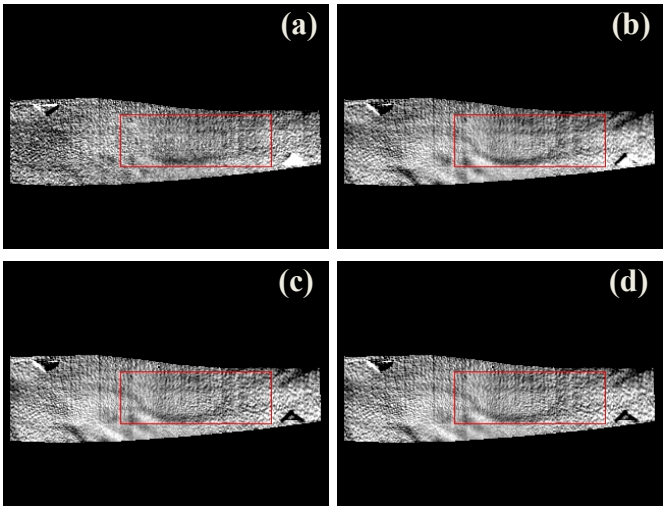

Fig. 6 TSR-images with the highest contrast (2 minutes occlusion, 4th order) (a) 2 Hz; (b) 5 Hz; (c) 10 Hz; (d) 20 Hz.

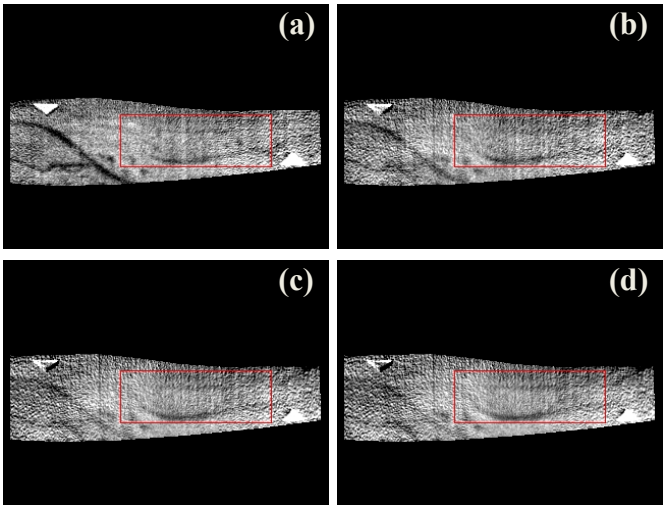

Fig. 7 TSR-images with the highest contrast (2 minutes occlusion, 5th order) (a) 2 Hz; (b) 5 Hz; (c) 10 Hz; (d) 20 Hz.

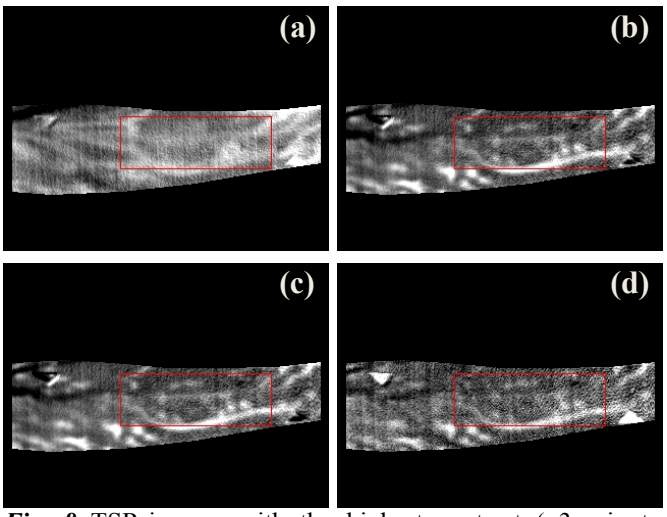

Fig. 8 TSR-images with the highest contrast (3 minutes occlusion, 4th order) (a) 2 Hz; (b) 5 Hz; (c) 10 Hz; (d) 20 Hz.

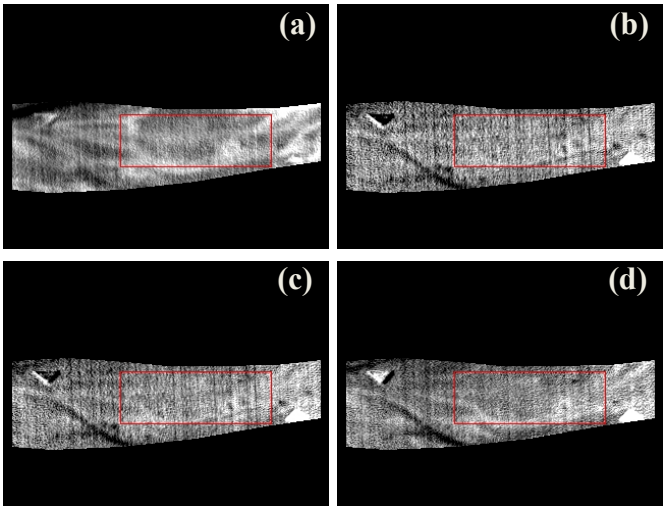

Fig. 9 TSR-images with the highest contrast (3 minutes occlusion, 5th order) (a) 2 Hz; (b) 5 Hz; (c) 10 Hz; (d) 20 Hz.

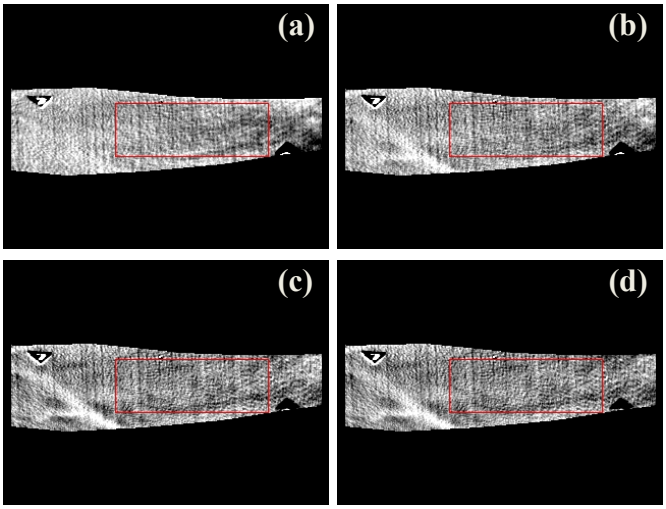

Fig. 10 TSR-images with the highest contrast (4 minutes occlusion, 4th order) (a) 2 Hz; (b) 5 Hz; (c) 10 Hz; (d) 20 Hz.

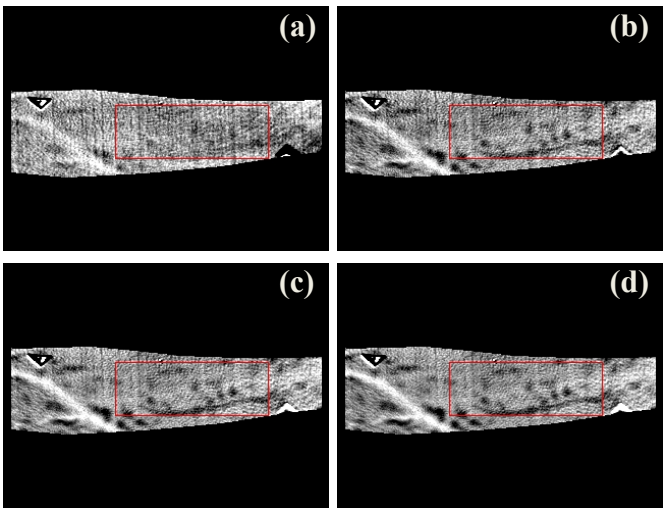

Fig. 11 TSR-images with the highest contrast (4 minutes occlusion, 5th order) (a) 2 Hz; (b) 5 Hz; (c) 10 Hz; (d) 20 Hz.

After TSR processing, the vascular patterns in each figure are generally clearer and less noisy except Figs. 9 and 10. By changing the order of polynomial fitting and occlusion period, we have 6 scenarios in total (Table 1-3) after TSR processing. However, only 5th order in Table 1 and 4th order in Table 3 showed a trend that contrast value increased with the sampling rate. It is still not clear if higher order of polynomial fitting is good or not.

II. Small window on the subject's arm

Unlike the above experiment, Figs 12, 13 and 14 showed the unprocessed IR images with the largest contrast calculated from a smaller red rectangle window focused on the microvasculature. The intensity in each set of sub-figures was in the same scale. The unit of the scale bar is temperature in Celsius.

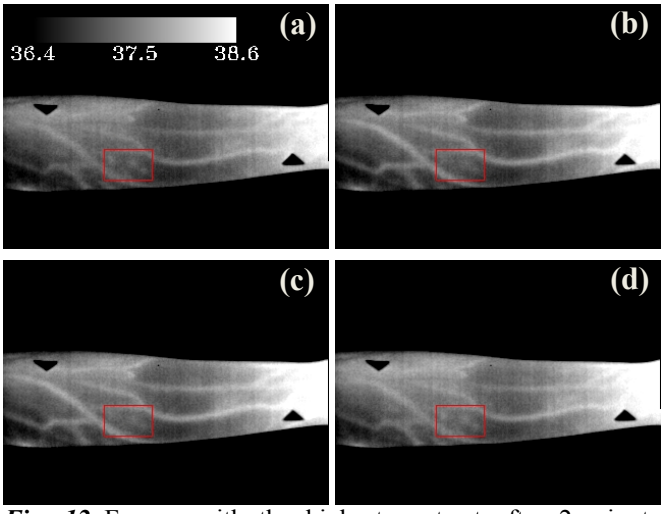

Fig. 12 Frames with the highest contrast after 2 minutes occlusion (a) 2 Hz; (b) 5 Hz; (c) 10 Hz; (d) 20 Hz.

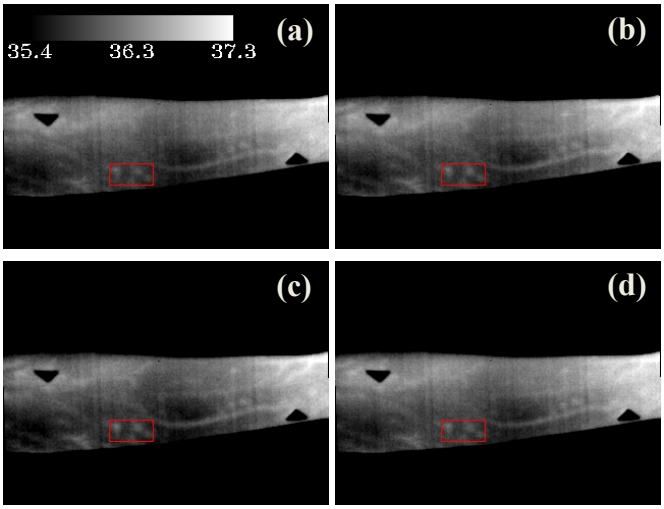

Fig. 13 Frames with the highest contrast after 3 minutes occlusion (a) 2 Hz; (b) 5 Hz; (c) 10 Hz; (d) 20 Hz.

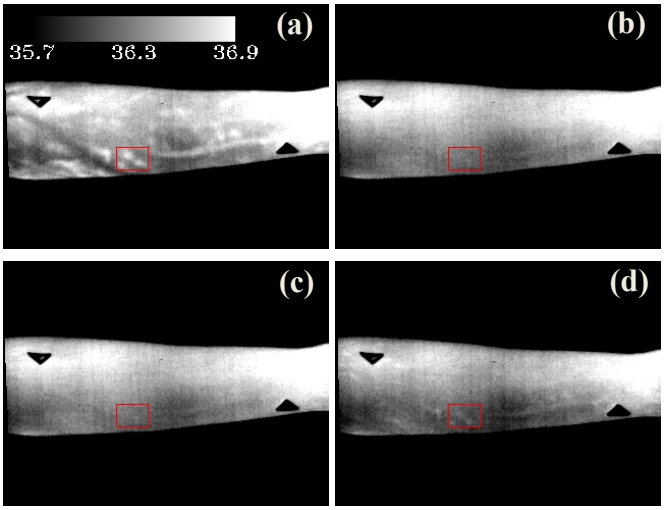

Fig. 14 Frames with the highest contrast after 4 minutes occlusion (a) 2 Hz; (b) 5 Hz; (c) 10 Hz; (d) 20 Hz.

By using a smaller window for contrast calculation we avoided the influence of sensor noise from the raw data. Comparing to Fig. 3 and 5, the contrast measure captured the vascular pattern in Fig. 12 and 14, but still missed the timing of maximum reactive hyperemia in Fig. 14 (b-c).

Table 4 The maximum contrast values and corresponding frame numbers after 2 minutes occlusion.

	Raw data	4th order	5th order
2 Hz	0.4902 (47)	0.9427 (3)	0.8729 (20)
5 Hz	0.5462 (242)	0.9370 (4)	0.9210 (21)
10 Hz	0.5692 (487)	0.9668 (24)	0.9519 (2)
20 Hz	0.6314 (515)	0.9910 (43)	0.9639 (20)

Table 5 The maximum contrast values and corresponding frame numbers after 3 minutes occlusion.

	Raw data	4th order	5th order
2 Hz	0.4166 (28)	0.8478 (9)	0.8867 (9)
5 Hz	0.4263 (93)	0.8313 (23)	0.9681 (31)
10 Hz	0.4755 (217)	0.8170 (42)	0.9394 (62)
20 Hz	0.5477 (299)	0.8512 (1)	0.9201 (112)

Table 6 The maximum contrast values and corresponding frame numbers after 4 minutes occlusion.

	Raw data	4th order	5th order
2 Hz	0.3024 (71)	0.9989 (7)	0.9989 (7)
5 Hz	0.3685 (71)	0.9996 (14)	0.9835 (10)
10 Hz	0.3685 (142)	0.9976 (24)	0.9902 (44)
20 Hz	0.4027 (339)	0.9967 (41)	0.9840 (80)

The reconstructed differential images (TSR-image) with the highest contrast were shown in Figure 15-20.

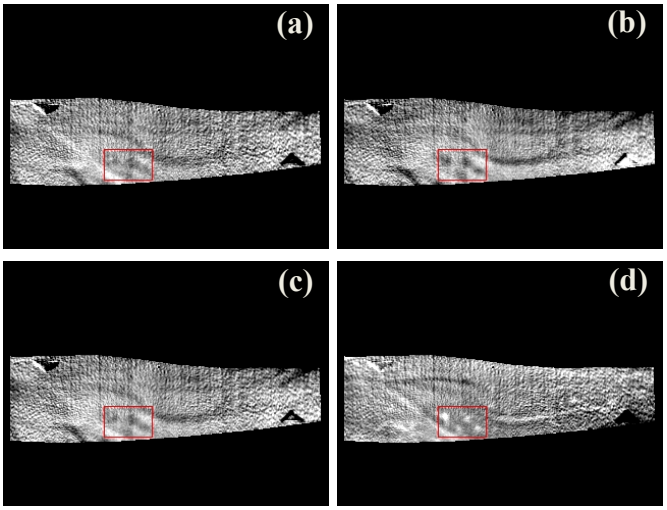

Fig. 15 TSR-images with the highest contrast (2 minutes occlusion, 4th order) (a) 2 Hz; (b) 5 Hz; (c) 10 Hz; (d) 20 Hz.

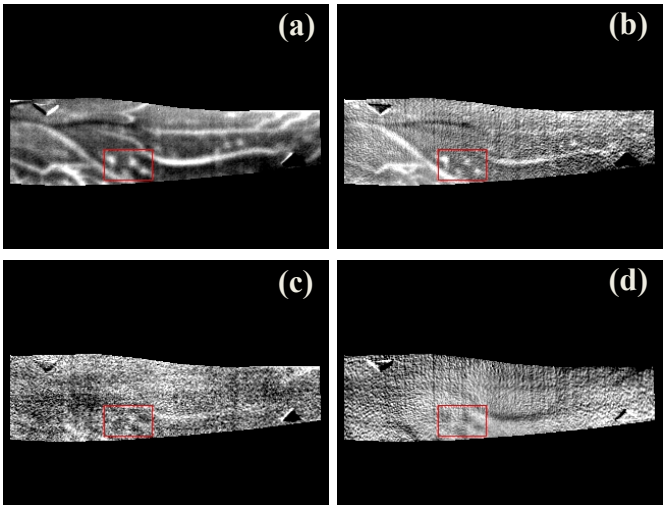

Fig. 16 TSR-images with the highest contrast (2 minutes occlusion, 5th order) (a) 2 Hz; (b) 5 Hz; (c) 10 Hz; (d) 20 Hz.

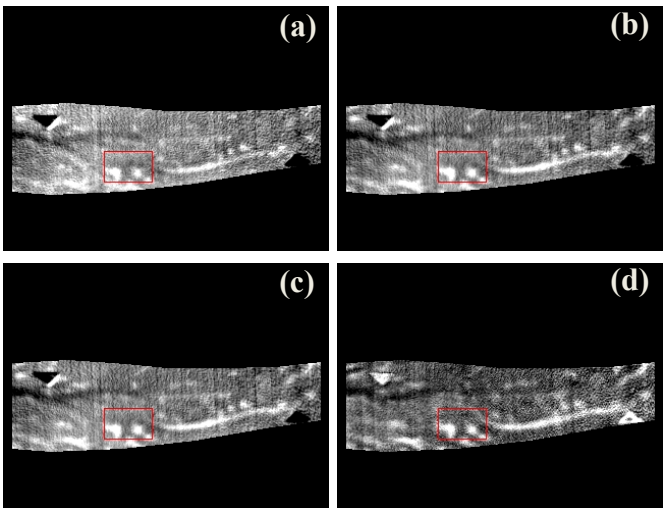

Fig. 17 TSR-images with the highest contrast (3 minutes occlusion, 4th order) (a) 2 Hz; (b) 5 Hz; (c) 10 Hz; (d) 20 Hz.

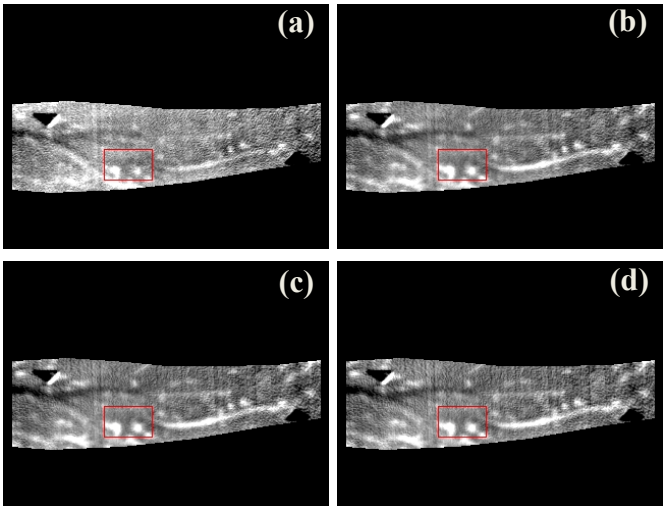

Fig. 18 TSR-images with the highest contrast (3 minutes occlusion, 5th order) (a) 2 Hz; (b) 5 Hz; (c) 10 Hz; (d) 20 Hz.

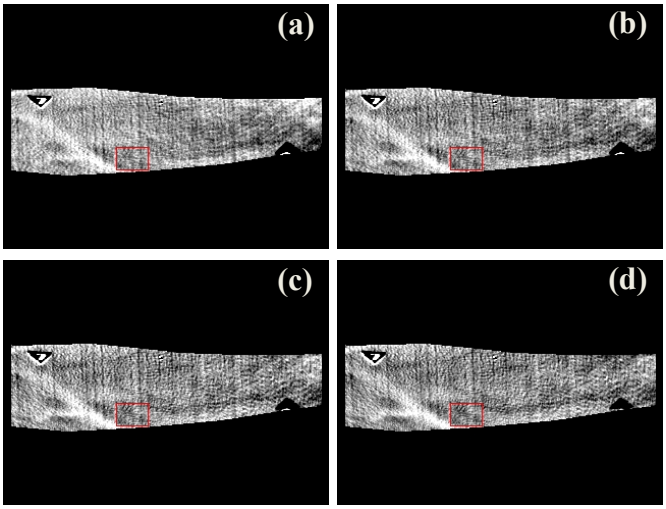

Fig. 19 TSR-images with the highest contrast (4 minutes occlusion, 4th order) (a) 2 Hz; (b) 5 Hz; (c) 10 Hz; (d) 20 Hz.

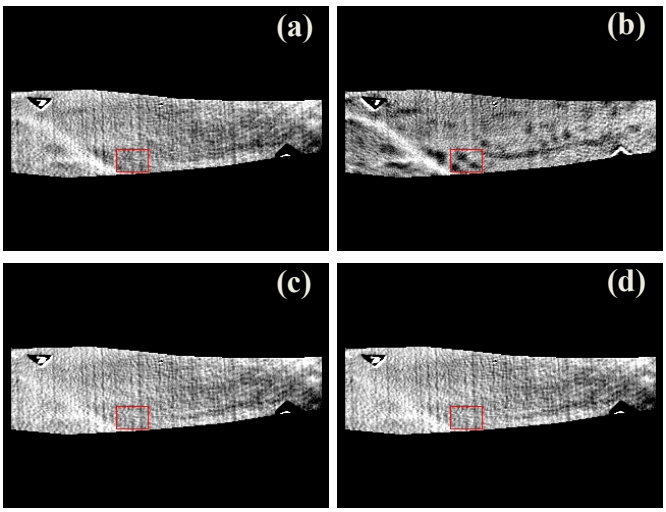

Fig. 20 TSR-images with the highest contrast (4 minutes occlusion, 5th order) (a) 2 Hz; (b) 5 Hz; (c) 10 Hz; (d) 20 Hz.

After TSR processing the two dot-like microvasculature can be seen in 3 minutes occlusion experiment (Figs. 17-18). Roughly five over eight scenarios (four sampling rates multiply two polynomial orders) in 2 minutes occlusion (Figs. 15-16) showed such pattern. Only one over eight scenarios in 4 minutes occlusion showed it, which again contradicted our assumption that 4 minutes occlusion induced the strongest response (Figs. 19-20).

B. Experiment 2 — Signal to noise ratio

In this experiment, we applied another measure, SNR, to quantify the results. We selected the red signal regions *(microvasculature)* and the blue noise/background regions *(skin)* marked in Fig. 21, and then calculated the SNR values according to equation (9).

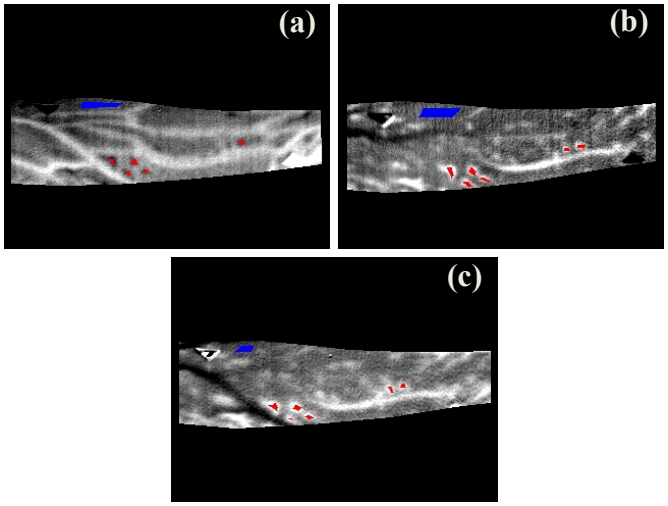

Fig. 21 The signal regions (*red ROI*) and background regions (*blue ROI*) for (a) 2 minutes; (b) 3 minutes; and (c) 4 minutes occlusion experiments.

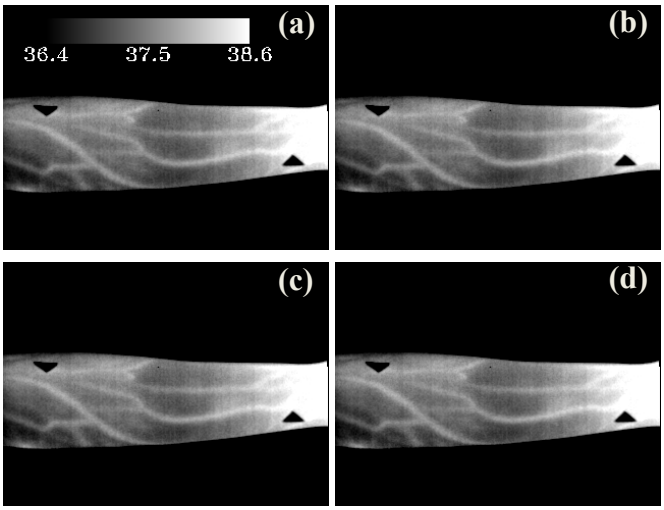

Fig. 22 Frames with the highest SNR value after 2 minutes occlusion (a) 2 Hz; (b) 5 Hz; (c) 10 Hz; (d) 20 Hz.

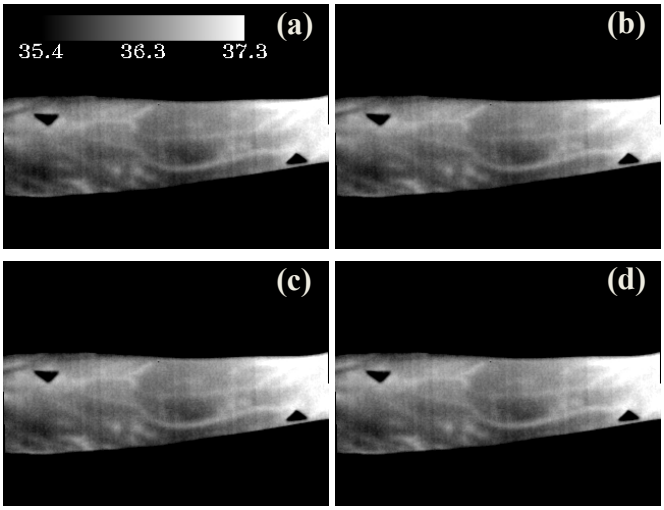

Fig. 23 Frames with the highest SNR value after 3 minutes occlusion (a) 2 Hz; (b) 5 Hz; (c) 10 Hz; (d) 20 Hz.

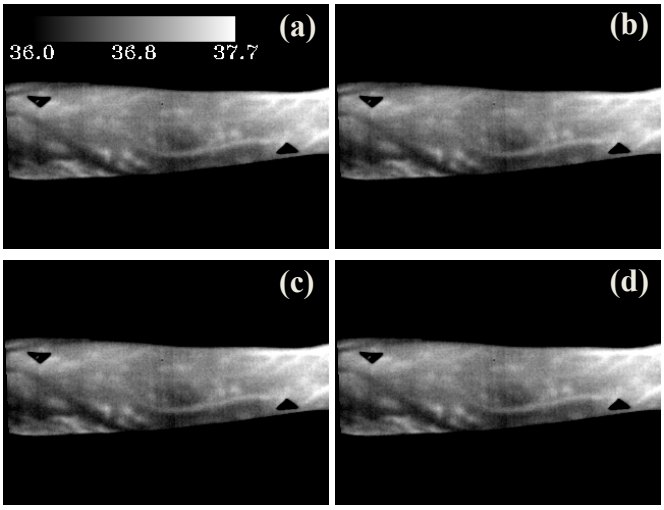

Fig. 24 Frames with the highest SNR value after 4 minutes occlusion (a) 2 Hz; (b) 5 Hz; (c) 10 Hz; (d) 20 Hz.

The above figures 22, 23 and 24 showed the raw IR images with the highest SNR values after 2, 3, and 4 minutes occlusion respectively.

Table 7 The maximum SNR values and corresponding frame numbers after 2 minutes occlusion.

	Raw data	4th order	5th order
2 Hz	-0.0566 (99)	22.7341 (16)	43.5500 (12)
5 Hz	-0.0549 (247)	33.8953 (36)	60.7265 (35)
10 Hz	-0.0534 (493)	42.4198 (72)	40.8556 (78)
20 Hz	-0.0532 (987)	52.1971 (147)	58.1882 (156)

Table 8 The maximum SNR values and corresponding frame numbers after 3 minutes occlusion.

	Raw data	4th order	5th order
2 Hz	-0.0522 (85)	42.4314 (34)	38.3499 (49)
5 Hz	-0.0513 (212)	56.7869 (68)	45.9393 (108)
10 Hz	-0.0497 (429)	63.1867 (118)	58.4573 (193)
20 Hz	-0.0497 (858)	65.8676 (215)	68.7114 (348)

Table 9 The maximum SNR values and corresponding frame numbers after 4 minutes occlusion.

	Raw data	4th order	5th order
2 Hz	0.0314 (86)	43.4367 (12)	40.2507 (80)
5 Hz	0.0315 (217)	38.9117 (26)	43.1573 (198)
10 Hz	0.0316 (433)	47.1558 (44)	55.1618 (69)
20 Hz	0.0316 (898)	53.3860 (83)	62.7201 (866)

The reconstructed differential images (TSR-image) with the clearest SNR value were shown in Figs 25-30.

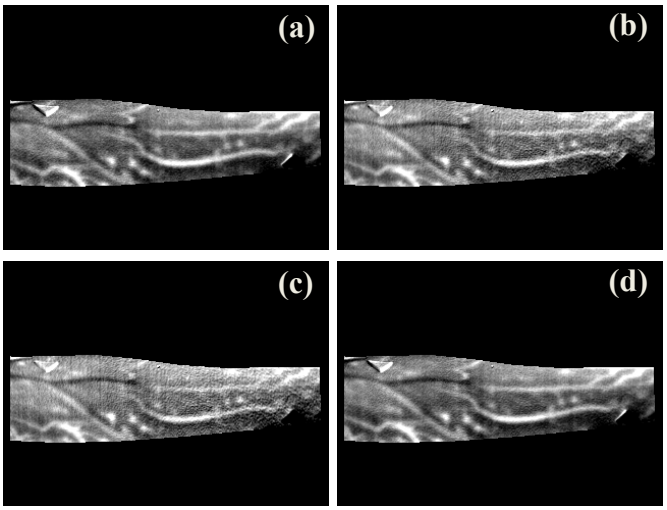

Fig. 25 TSR-images with the highest SNR value (2 minutes occlusion, 4th order) (a) 2 Hz; (b) 5 Hz; (c) 10 Hz; (d) 20 Hz.

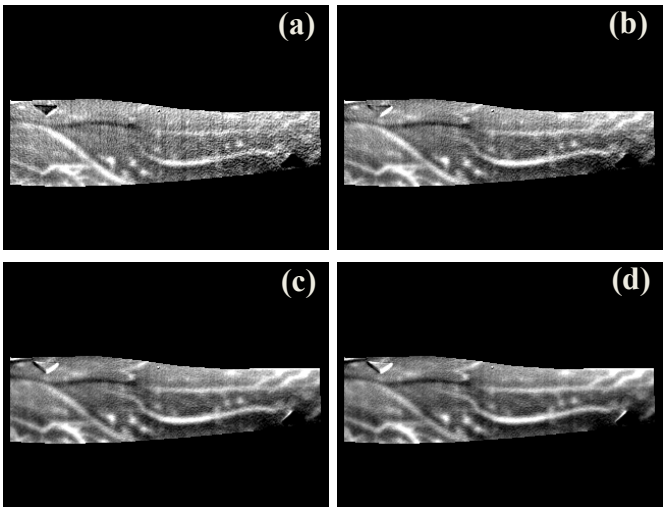

Fig. 26 TSR-images with the highest SNR value (2 minutes occlusion, 5th order) (a) 2 Hz; (b) 5 Hz; (c) 10 Hz; (d) 20 Hz.

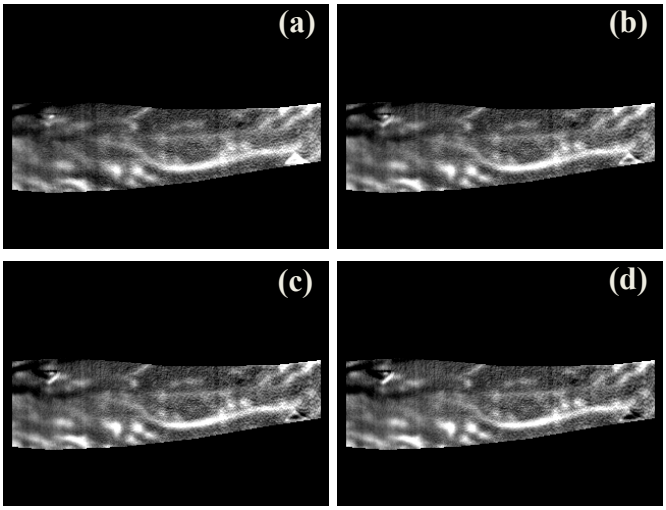

Fig. 27 TSR-images with the highest SNR value (3 minutes occlusion, 4th order) (a) 2 Hz; (b) 5 Hz; (c) 10 Hz; (d) 20 Hz.

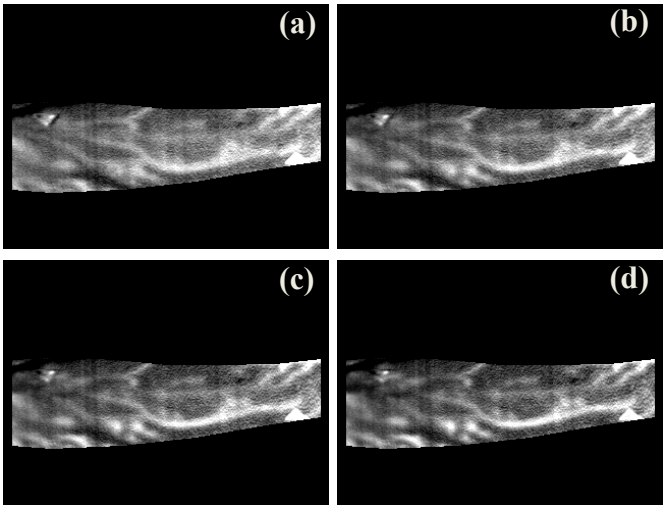

Fig. 28 TSR-images with the highest SNR value (3 minutes occlusion, 5th order) (a) 2 Hz; (b) 5 Hz; (c) 10 Hz; (d) 20 Hz.

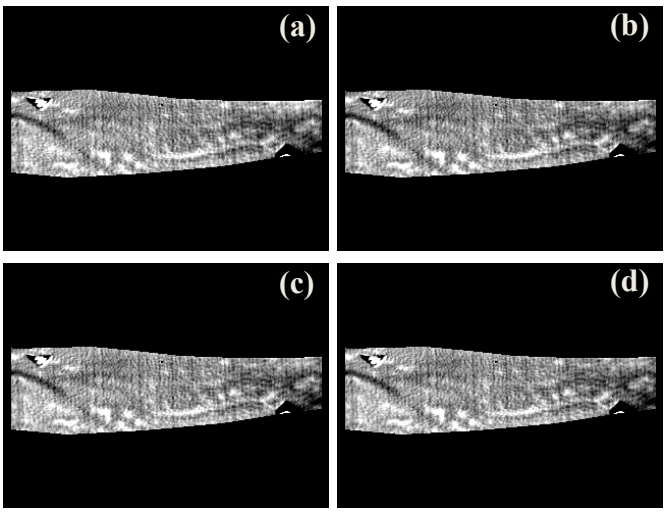

Fig. 29 TSR-images with the highest SNR value (4 minutes occlusion, 4th order) (a) 2 Hz; (b) 5 Hz; (c) 10 Hz; (d) 20 Hz.

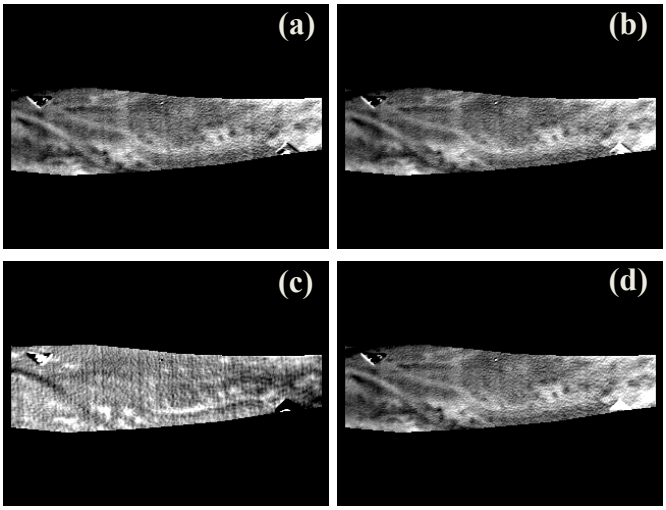

Fig. 30 TSR-images with the highest SNR value (4 minutes occlusion, 5th order) (a) 2 Hz; (b) 5 Hz; (c) 10 Hz; (d) 20 Hz.

Comparing to section III. A, which showed frames with the highest contrast value, we found that generally SNR could help us to select the TSR-processed images with clear vascular and microvascular patterns. It performed well in 2- and 3-minute occlusion experiments (Figs. 25-28), and did not do well in 4 minutes occlusion experiment. It is possible that the data quality of 4 minutes occlusion is not as good as the other two experiments.

IV. DISSCUSSION AND CONCLUSIONS

According to the experimental results, we found that TSR approach could greatly enhance the image contrast between different tissues. It is particularly useful when locating vasculature smaller than the conduit vessels. However, the contrast measure used in previous study [6] failed in reporting images compatible with human perception, no matter what size of the window was. The quantification results were inconsistent under different scenarios, and the result images with the highest contrast are not helpful in locating microvasculature particularly for scenarios with large window. The main reason could be that the raw data was too noisy due to the physical characteristics of the microbolometer sensor.

To overcome this problem, we adopted another well-known quantification method — ***S***ignal-to-***N***oise ***R***atio (*SNR*). By using this method, we could observe that after 4th order TSR processing the SNR values increased with the sampling rate. The SNR values in 5th order did not follow such trend completely, which could be resulted from its higher fitting capability that also smoothes the temporal variation in each pixel. The corresponding frame numbers also showed that we could observe the microvasculature much earlier in TSR-processed image series than in the raw images. Such information helps us in determining the response period of reactive hyperemia induced by the occlusion experiment.

We conclude that the study focused on exploring the relationship between the temporal resolutions (image acquisition rate) and the quality of TSR-reconstructed images.

When applying TSR processing for tissues enhancement we found that higher sampling rate is generally helpful in terms signal to noise ratio as well as the human perception. The order of polynomial fitting seems to have certain optimal value which depends on various conditions such as surrounding environment, subjects, duration of study, or sensitivity of camera. Higher order is not always preferred.

ACKNOWLEDGMENT

We appreciate Dr. Alexander Gorbach from National Institute of Health, USA for his support on the testing data and the insightful discussions. The research is funded by National Science Council of Taiwan, Republic of China (NSC 101-2221-E-194-018).

REFERENCES

[1] Zeman HD, Lovhoiden G, Vrancken C, Danish R., "Prototype vein contrast enhancer," Optical Engineering 2005;44:086401.

[2] Verdaasdonk RM, de Roode R, de Vooght KM, Viergever MA, Kalkman CJ, de Graaff JC, "Visualizing Veins With Near-Infrared Light to Facilitate Blood Withdrawal in ChildrenCuper NJ," Clin Pediatr (Phila). 2011 Jun;50(6):508-12.

[3] S. Bagavathiappan, T. Saravanan, John Philip, T. Jayakumar, Baldev Raj, R. Karunanithi, T. M. R. Panicker, M. Paul Korath, and K. Jagadeesan1 "Infrared thermal imaging for detection of peripheral vascular disorders," J Med Phys. 2009 Jan-Mar; 34(1): 43–47.

[4] S. A. Feig, "Thermography, Mammography, and Clinical Examination in Breast Cancer," Radiology vol 122 January 1977, 123-127.

[5] A. M. Gorbach, *et al*., "Infrared imaging of nitric oxide-mediated blood flow in human sickle cell disease," Microvascular Research, vol. 84, no. 3, pp. 262-269, Jul. 2012.

[6] W. Liu, J. Maivelett, G.J. Kato, *et al*., "Reconstruction of Thermographic Signals to Map Perforator Vessels in Humans," Quantitative Infrared Thermography Journal, 2012. 9(2): p. 123-133.

[7] Shepard, S.M., *et al*., "Reconstruction and enhancement of active thermographic image sequences," Optical Engineering, 2003. 42(5): p. 1337-1342.

[8] Beghdadi, A. and A. Le Negrate, "Contrast enhancement technique based on local detection of edges," Computer Vision, Graphics, and Image Processing, 1989. 46(2): p. 162-174.